Effect of fibers on the temperature field and radial deformation behaviour of self-compacting concrete pipes under cyclic fire condition

Genjin LIU[a], Yining DING[a]*, Yuehua WANG[b], Yulin ZHANG[c]

[a] State Key Laboratory of Coastal and Offshore Engineering, Dalian University of Technology, Dalian 116024, China

[b] Dalian Institute of Building Scientipc Research & Design Stock Co..LTD, Dalian 116021, China

[c] University of Minho, Centre of Mathematics, Braga 4700-052, Portugal

Abstract: In this paper, the radial deformation of fiber reinforced self-compacting concrete (SCC) pipes under cyclic fire conditions is studied. A series of experimental study on the temperature fields and radial deformation properties of steel mesh, polypropylene fiber (PP fiber) and macro steel fiber (SF) reinforced SCC pipes subjected to fire is carried out. A novel method for measuring the deformation of pipes under high temperature has been proposed. The results indicate that both micro PP fiber and macro SF are effective in decreasing the temperature difference and reducing the radial deformation in each thermal cycle. A significant positive synergistic effect on decreasing the residual radial deformation can be achieved by combined use of macro SF and micro PP fiber. The elastic theory is used to estimate the elastic portion in the total radial deformation, and the elastic radial deformation is about 22.3% of the maximum radial deformation in the first thermal cycle. Based on the elastic

calculation and observed experimental results, a simplified method for estimating the maximum radial deformation in the first thermal cycle is proposed.

Keywords: Temperature-time curve; radial deformation; cyclic heating; fiber reinforced SCC pipes

1. Introduction

Fiber reinforced concrete (FRC) has been increasingly used in many civil engineering structures such as high-rise buildings, bridges, highway and pipes[1-4]. Fire accidents in pipe for underground structure like pipe gallery (for gas, heat, electricity and communication) lead to high heating rates and the temperatures often exceeding 1000 ℃, which may result in severe damage to concrete. Usually the underground structure is connected to other facilities, wherever a fire breaks out, it spreads rapidly to another location. Therefore studies on the FRC pipe members under the fire condition become more and more important, as it is directly related to the safety of the structures and human lives.

Numerous studies[5-10] were conducted on the physical, mechanical behavior and fire properties of concrete or FRC, and they are mainly concentrated on the mechanical strength, toughness and the microstructure change before or after high temperature. The macro steel fiber (SF) reinforced concrete shows higher flexural toughness and ultimate load before high temperatures, but micro polypropylene fiber (PP Fiber) does not show a clear effect on the mechanical properties of concrete[11]. Some investigations[12, 13] focus on the mechanical behavior of the FRC pipe elements and find that the steel and synthetic fibers reinforced concrete pipes seem to be economical and effective alternatives to the classically-reinforced-concrete pipes.

Some scholars focus on the spalling behavior of concrete or FRC under high temperature [1, 14, 15]. In order to reduce the risk of concrete spalling and enhance the high-temperature resistance ability, PP fiber and SF are added into concrete. Bangi[1] points out that the addition of PP fiber is very effective in mitigation of spalling and addition of steel fibers plays some role in pore pressure reduction at relatively higher pressures in deeper regions of concrete. In addition, the composed use of PP fiber and SF shows a clear positive effect on the pore pressure reduction subjected to fire[16] and better mechanical properties during and after exposure to elevated temperatures compared to plain and mono-fiber mixtures[1].

The fire resistance of aboveground FRC structure members (slabs[17], columns[18], corbels[19] and beams[20]) (heat transfer flows multidirectionally) is investigated in previous studies. But the consequences can be extremely destructive and dangerous if a fire occurs in underground structures (heat transfer always flows in one direction), especially for a pipe member, because the enclosed space hinders the dissipation of heat and smoke[21]. Several tests have been developed to investigate the thermal and mechanical behavior of FRC specimen during and after high temperature exposure, including the stress and strain, thermal expansion or cracking and spalling behavior [22-24]. However, they are carried out in the electrical furnace, which offers a relatively uniform temperature distribution around the structural members. The temperature field under fire of underground structures is much more severe than that in electrical furnaces. Also, the study on the behavior of underground FRC structure member under fire, especially on the radial deformation of pipe element subjected to fire, is still very limited. One of the key challenges is the difficulty of the acquisition of the deformation data under the fire condition due to the low working temperature of commonly used linear variable differential transformer (LVDT, traditionally metallic based LVDT-usually only up to 85 ℃). Therefore, a new type of high-temperature LVDT (HTLVDT), which can measure the deformation under the temperature up to 1200 ℃, has been invented for investigating the deformation under high temperature.

The pipe members may experience many prolonged cycles of high temperatures. The objectives of fire-resistant FRC pipe member under fire include a number of issues such as the heat-transfer mechanisms, spalling behavior, cracking and smoke spread, manufacturing and material properties [25-27]. However, it is not intended in this study to present a complete knowledge of every aspect of the FRC pipe.

The focus of this paper is given to investigating the fiber effect on the temperature field of pipe section and radial deformation behavior in the self-compacting concrete (SCC) pipe members during one and two cyclic fire loading. The steel mesh, micro PP fiber and macro SF, as well as the combined use of PP fiber and SF are employed in this study. Influence of steel mesh, mono fiber and hybrid fibers on the temperature-time relationship, temperature difference, maximum radial deformation and residual radial deformation of the pipes are investigated. In addition, the relationships between the radial deformation and the temperature, the radial deformation and the temperature difference of the pipes are also studied. In order to estimate portion of the elastic radial deformation compared to the

total radial deformation and to evaluate the maximum radial deformation, a simplified method is suggested based on the elastic calculation and observed experimental results.

2. Experimental program

2.1. Materials

The base mix design of the concrete without fiber reinforcement is illustrated in Table 1. The concrete is made with P•II 42.5R Portland cement and class C fly ash. The coarse aggregates are crushed limestone gravel, with a particle size between 5 and 12 mm. The fine aggregates are natural river sand and have fineness modulus of 2.46, with a particle size of 0-5 mm. The PP fiber and SF are added into the concrete, see Fig. 1. The parameters of different fibers are illustrated in Table 2.

Table 1 Base mixture proportion of plain concrete (kg/m^3)

Cement	Fly ash	Fine aggregate (0-5 mm)	Coarse aggregate (5-12 mm)	Water	Superplasticizer	Water/Binder
500	100	764	764	222	3.5	0.37

Table 2 Properties of steel fiber and polypropylene fiber

Fiber	Length (mm)	Diameter(mm)	Tensile stress(MPa)	Pieces for per kilogram	Melting Point(℃)
PP fiber	15	0.03	400	2×10^7	165
SF	35	0.55	1200	15000	1500

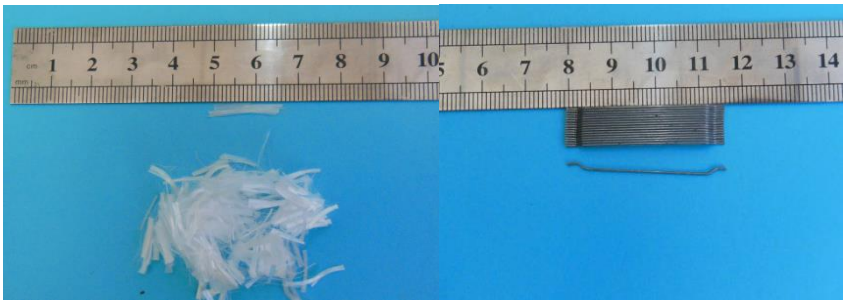

(a) (b)

Fig. 1 Fibers used in this study (a) Micro PP fiber; (b) Macro steel fiber.

2.2. Pipe specimens and test setup

Nine concrete pipes are prepared for the tests. The inner radius of the FRC pipe is 200 mm, the outer radius is 250 mm, and the thickness is 50 mm. The fiber dosages for the specimens and the slump flow are shown in Table 3. The slump flow tests are carried out according to EFNARC 2002[25]. In Table 3, RC refers to the self-compacting concrete pipe specimen without any fiber but with steel mesh reinforcement. The steel mesh with a reinforcement ratio of 0.4% is used. The steel mesh is produced by hot-rolled rebar, with a diameter of 6 mm and bar spacing 15 cm. PP1 means specimen with 1kg/$m^3$of PP fiber; HF403 implies the specimen hybrid with 40 kg/m^3 SF and 3 kg/m^3 PP fiber. The specimens are cast in a steel mold. After demolding, the specimens are moved to the curing room at a temperature of 20±2 ℃ and humidity of about 95% for 28 days.

Table 3 Fiber dosages, slump flow and compressive strength of FRC

Specimen	PP fiber(kg/m^3)	SF(kg/m^3)	Slump flow(cm)	Compressive stress(MPa)
RC	0	0	68	43.6
PP1	1	0	55	38.9
PP3	3	0	39	37.6
SF40	0	40	64	48.2
SF55	0	55	62	47.5
SF70	0	70	59	45.9
HF403	3	40	37	38.1
HF552	2	55	48	41.9
HF701	1	70	52	42.6

The test set-up is shown in Fig. 2. The cross-section of the specimens and measuring position are shown in Fig. 2a. As shown in Fig. 2b, the pipe specimen is set up on the platform through which the gas fire can be led into the pipe. The end of each pipe is fixed with a pedestal. The temperatures of the gas and the different layers of the pipe are measured by a high temperature thermocouple, and the

radial deformations of the pipe in four directions are measured by the self-designed HTLVDT. The invented HTLVDT is characterized by using a chrome nickel steel bar with low heat-conductive parameter and low heat expansion parameters as an extending section of the traditional metallic LVDT[29]. The average value of the four HTLVDT is adopted as the radial deformation for the pipes. The section of the measured points is 600 mm from the exit of the gas line. The test set up is illustrated in Fig. 3.

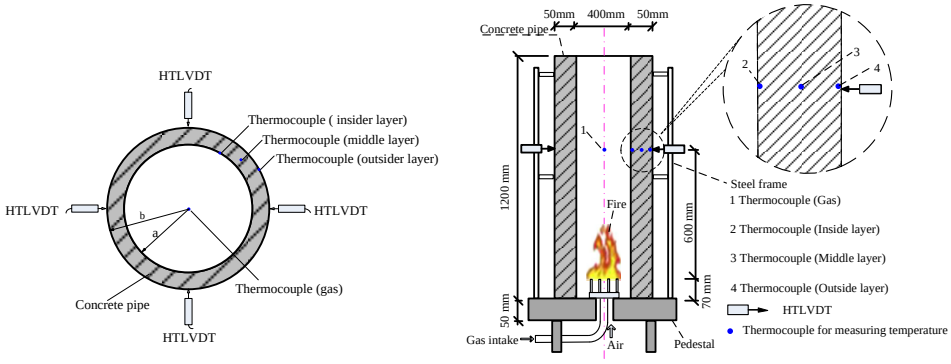

(a) (b)

Fig. 2 (a) Cross-section of the specimen and measuring position; (b) Vertical section of the testing set-up and measuring position.

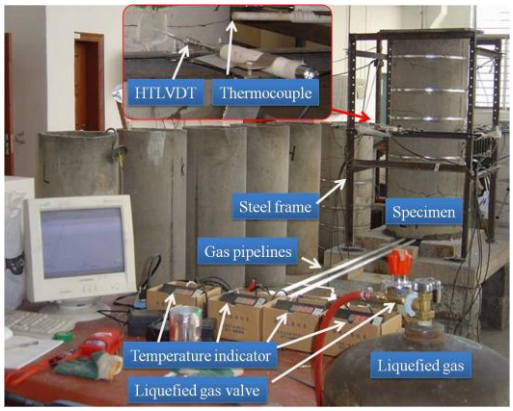

Fig. 3 Test set-up.

The temperature - time (T-t) curve is the precondition for analyzing the temperature field and can

significantly reflect the deformation performance of the pipe under fire. Literature [30] demonstrates that the T-t curves in tunnels are usually more severe than those T-t curves mainly used in buildings such as ISO 834[31] and EN 1363[32] and so on. Thus, the two-circle thermal test is carried out based on guideline UNI EN 13216-1: 2006[33]. The thermal cycle of the pipe is controlled by the gas temperature and is divided into two similar stages. As shown in Fig. 4, the heating rate is 100 ℃/min, the temperature of the gas increases up to 1000 ℃ in 10 mins, after that it remains stable about 30 mins at 1000 ℃, then it falls down naturally to room temperature. The second cycle is the same as the first one. In addition, the tests were carried out without mechanical load but only with dead load of the specimen.

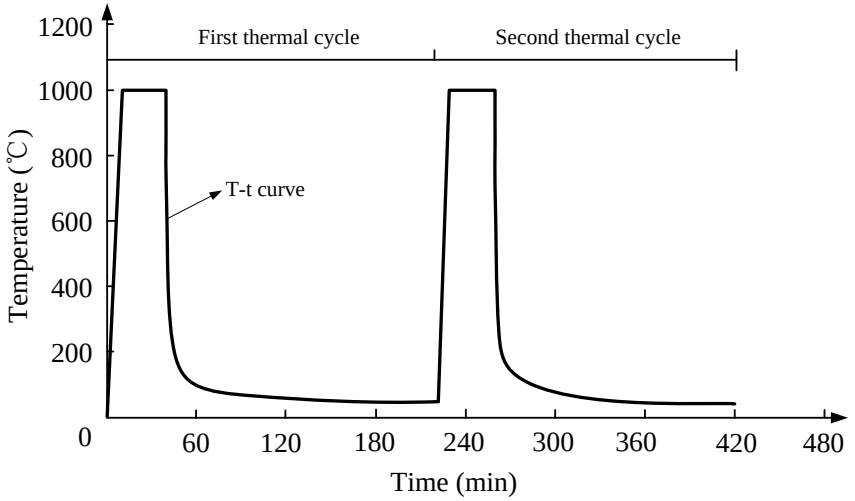

Fig.4. Temperature - time curve.

3. Experimental results and theoretical analysis

3.1. Experimental results

3.1.1 Effect of fibers on the compressive strength

In order to investigate the effect of the fibers on the compressive strength, uniaxial compression test is carried out on prism specimens of 150×150×300 mm. The mean values of the compressive strength of 3 specimens after 28 days are given and compared in Table 3. It can be concluded that the compressive strength decreases by a maximum of 13.8% by the addition of PP fibers.

3.1.2 Effect of fibers on temperature difference (Δ_T) of the pipe cross section during two thermal cycles

The temperature-time curves of the heated gas, the inside layer, the middle layer and the outside layer of the steel mesh reinforced self-compacting concrete (RC) pipes, SF, PP fiber and hybrid fiber reinforced concrete pipes are illustrated in Fig.5, Fig.8 and Fig.9. In the thermal cycles, the temperature decreases from the inside layer to the outside layer gradually during the heating and the natural cooling stages. Furthermore, the temperatures of the inside layer, the middle layer and the outside layer reach the maximum value at the beginning of the decrease in the gas temperature.

3.1.2.1 Effect of PP fiber on the temperature difference (Δ_T) of SCC pipe

The peak values of temperature difference (Δ_T) in the first thermal cycle between the inside layer and the outside layer of RC, PP1 and PP3 are 307, 343 and 311 ℃, respectively. In the second thermal process, the peak values of Δ_T are 311, 364 and 307 ℃, respectively. Compared with PP3, the maximum Δ_T of PP1 decreased by 10.3% in the first thermal cycle and decreased by 18.6% in the second thermal cycle. This illustrates that with the increasing of PP fiber content, the Δ_T between the inside and outside layer is reduced. It is due to the melting of PP fibers, a connected network is constituted and the network is more permeable than the concrete matrix[34]. The role of PP fibers is to create a connected network for the transfer of thermal fluids (See Fig. 6). It is known to all that heat transfer is classified into various mechanisms, such as thermal conduction, thermal convection and thermal radiation. When PP fibers are melted under high temperature, the thermal conduction mechanism will be changed to thermal convection in the continuous microchannels. In addition, the more microchannels in the matrix under high temperature field, the faster the thermal convection will be. Therefore, the temperature difference of PP3 is smaller than that in PP1.

During the two thermal cycles of PP1 specimen, the maximum temperature difference (Δ_T) between the inside and outside layer is higher than that of RC, due to the thermal conductivity coefficient of PP fibers and the air-filled pores are lower than that of steel mesh. (λ_s is about 54 W/m℃, $\lambda_{polypropylene}$ is

about 0.24W/m℃, λ_{air} is about 0.024 W/m℃). However, with the increase of PP fiber content (from 1kg/m^3 to 3kg/m^3), the maximum Δ_T of PP3 is close to that of RC. The results indicate that micro PP fibers are effective in decreasing the temperature difference of SCC pipes.

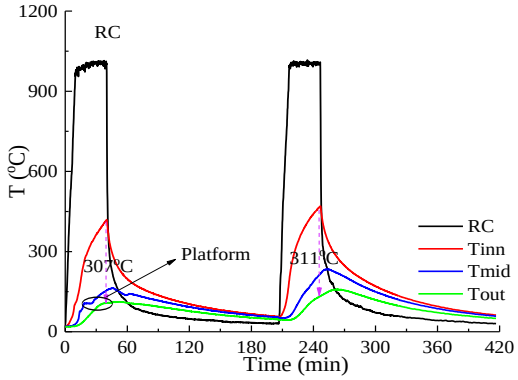

(a)

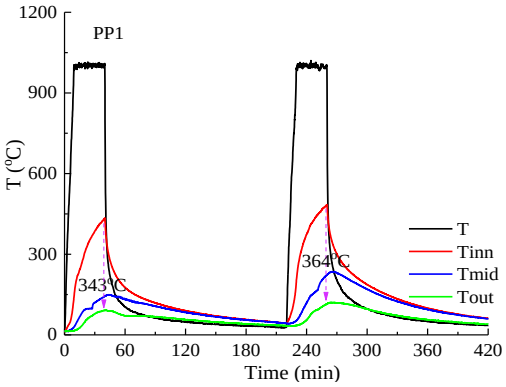

(b)

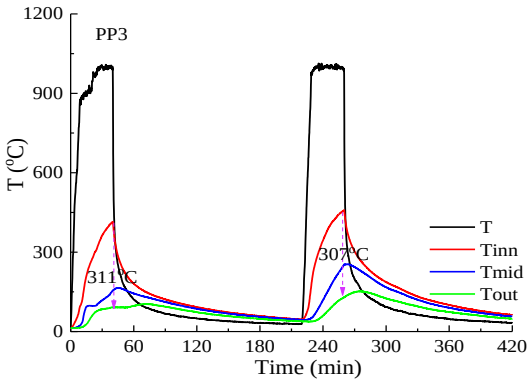

(c)

Fig. 5 Temperature-time curves of the heated gas, the inside layer, middle layer and outside layer of the PP fiber reinforced pipes (a) RC; (b) PP1; (c) PP3.

As illustrated in Fig.5, there is a plateau on the temperature-time curve of the middle layer during 18 - 27 min. For example, the middle layer temperature rise of RC specimen exhibits the plateau during 18-25 min which starts above 100 ℃ and ends at 106.7 ℃, with the heated gas temperature varying from 986.6 to 1009.2 ℃. This platform implies a delay of temperature increase caused by the water evaporation in concrete (see Fig. 7), which is an energy-consuming and transformation progress.

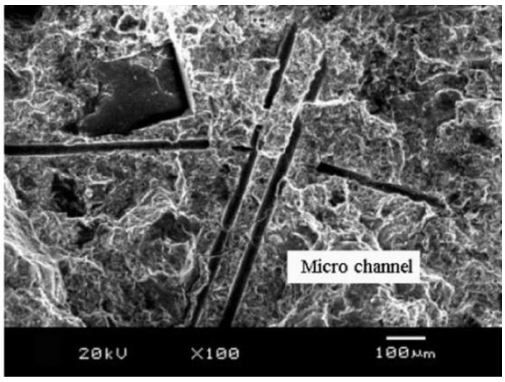

Fig.6. Micro channels in concrete matrix due to melting of PP fibers [11].

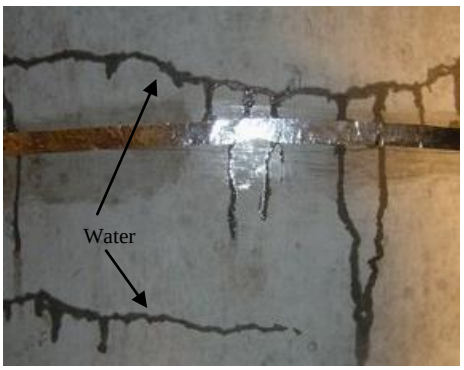

Fig. 7 Water evaporation.

3.1.2.2 Effect of SF on the temperature difference (Δ_T) of SCC pipe

It also can be found in Fig.8 that the temperature reduces from the inside layer to the outside layer gradually across the pipe section. In the two thermal cycles, the temperature of inside layer reaches its

peak value at the beginning of the decrease in the gas temperature, as shown in Fig. 8a), 8b) and 8c), and the variations of the pipe's temperatures lag behind the variation of the gas temperature.

In the first thermal cycle, the maximum temperature difference Δ_T between the inside layer and the outside layer of SF40, SF55 and SF70 is 338, 318 and 279 ℃, respectively. In the second cycle, the maximum Δ_T of SF40, SF55 and SF70 is 351, 323 and 279 ℃, respectively.

Compared with SF40, the maximum Δ_T between the inside layer and outside of SF55 and SF70 decreased by 5.9% and 17.4% in the first cycle, and for the second cycle, the decrement is 8.0% and 17.7%, respectively. It demonstrates that with the increase of SF content, the maximum Δ_T between inside layer and outside layer decreases significantly, because the thermal conductivity of SF are much higher than that of concrete ($\lambda_{concrete}$ is about 1.0-2.0 W/m℃). For RC, the steel content is equivalent to 62 kg/m^3, the measured maximum Δ_T is 307°C in first thermal cycle. It can be seen that the reinforcement degree of RC specimen is between SF55 and SF70, and the measured Δ_T (307 °C) of RC is also between SF55 (318 °C) and SF70 (279 °C). In addition, the same conclusion can be drawn in the second thermal cycle. This is what was expected, it means the test results confirm with above analyses.

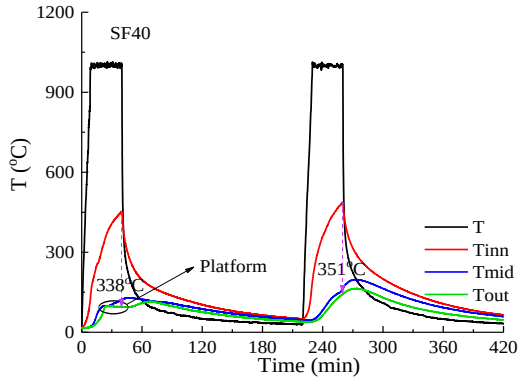

(a)

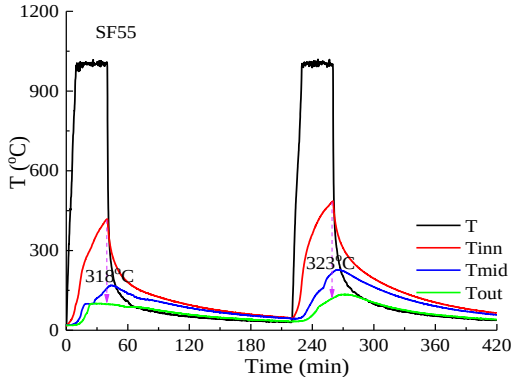

(b)

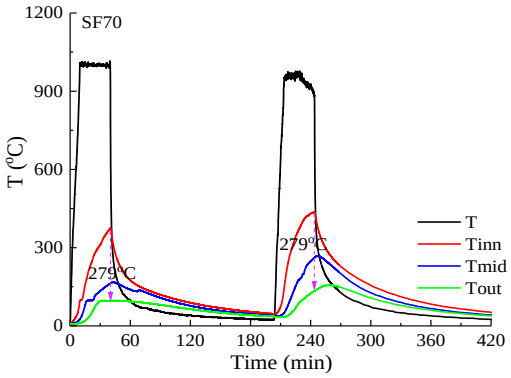

(c)

Fig. 8 Temperature-time curves of the heated gas, the inside layer, the middle layer and the outside layer of the SF reinforced pipes (a) SF40; (b) SF55; (c) SF70.

3.1.2.3 Effect of hybrid fibers on the temperature difference (Δ_T) of SCC pipe

For hybrid fiber reinforced pipe specimens in Fig.9, the Δ_T between the inside layer and outside layer of HF403, HF552 and HF701 is 349, 295 and 242 ℃, for respectively. In the second thermal test, the Δ_T is 319, 297 and 281℃, respectively. With the increasing of SF content (from 40 to 70 kg/m^3) and decreasing of PP fiber content (from 3 to 1 kg/m^3), the maximum Δ_T decreases.

Moreover, in terms of the maximum Δ_T between the inside and outside layers, HF403 is smaller than SF40 meanwhile HF552 is smaller than SF55. In addition, the maximum Δ_T of HF701 is smaller than that of SF70 and PP1 in both thermal cycles. It can be traced back to that the high content of hybrid fibers may provide a more uniform temperature field under fire than that of the mono SF and PP fiber.

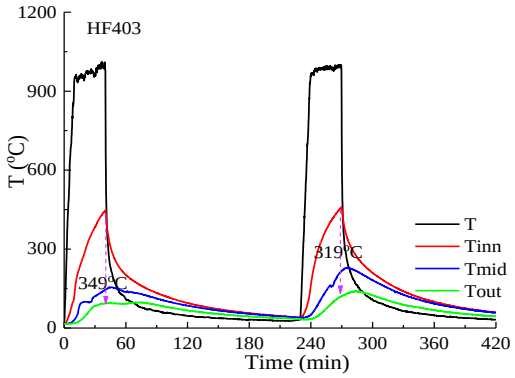

(a)

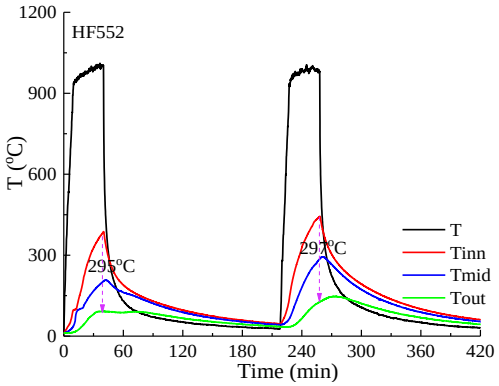

(b)

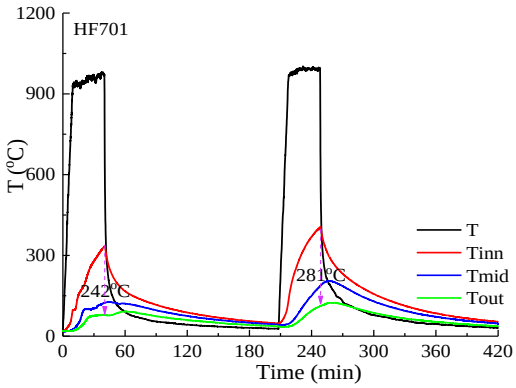

(c)

Fig. 9 Temperature-time curves of the heated gas, the inside layer, the middle layer and the outside layer of the hybrid fiber reinforced pipes (a) HF403; (b) HF552; (c) HF701.

3.1.3 Effect of different fibers on the radial deformation of SCC pipes

3.1.3.1 Effect of PP fiber on the radial deformation (d_r) of SCC pipes

Fig. 10 shows the comparison of the radial deformation-time curves of SCC pipes reinforced with PP fiber and steel mesh. It can be seen that the radial deformation (d_r) of PP fiber reinforced pipes increases more rapidly than that of steel mesh reinforced pipes during the first heating process. The maximum d_r of the pipe is equal to its first peak value at about 40 min. It means that d_r reaches the maximum at the beginning of the decrease in the gas temperature (about 1000 ℃).

The maximum d_r (δ_{m1}, δ_{m2} are the maximum d_r of the pipes in the first and second thermal cycle respectively) and residual d_r (δ_{r1}, δ_{r2} are the d_r of the pipes at the end of first (210 mins) and second (420 mins) thermal cycle respectively) of the pipes are listed in Table 4. Compared with RC pipe, in the first thermal cycle, the δ_{m1} of PP1 and PP3 are increased by 51.8% and 18.8%, respectively. It can be seen that with the increasing of PP fiber content, the δ_{m1} of the pipe decreases. During the second thermal cycle, the δ_{m2} of PP1 and PP3 pipes is 2.14 mm and 1.67 mm, respectively. These two values are 65.9% and 65.3% higher than the corresponding values of the peak radial deformation (δ_{m1}) in the first cycle. It is observed that the maximum d_r can be decreased by the addition of PP fiber. Indeed, there is another point worth mentioning here, the δ_{m2} of PP3 is 45.2% higher than that of steel mesh reinforced pipes. It means that the steel mesh (steel ratio of 0.4%) used in this test possesses a better confining ability of radial expansion than that of 3 kg/m^3 PP fiber.

At the end of the first cooling stage (at 210 min), the δ_{r1} of the PP3 pipe is 0.32 mm, which is 28.9% less than that of the PP1 and 5.9% less than that of RC specimen, respectively. After the second thermal cycle, the δ_{r2} of PP1 and PP3 is accumulated to 0.91 mm and 0.86 mm, respectively. With the increasing of PP fiber content, the δ_{r2} of the pipe is also decreased. It means that the PP fiber has a positive effect in reducing the residual radial deformation. Indeed, PP3 shows a higher δ_{r2} than that of RC pipes. The results illustrate that the restraining effect of 3 kg/m^3 PP fiber on the residual deformation is less than that of the steel mesh. There may be two reasons: the first is that the micro PP fiber as a non-structural material can hardly restrain the deformation after cracking; the second reason is that most of the PP fibers are melt during the two thermal cycles.

After two thermal cycles, δ_{r2} of PP1 and PP3 is about 2.0 folds and 2.7 folds of δ_{r1}, respectively. The unrecovered d_r is increased due to the crack propagation during the thermal process. For steel mesh reinforced RC pipe, the residual d_r is about 40% of the maximum d_r in each cycle. For PP fiber reinforced pipe, the ratio of residual d_r to the maximum d_r is between 31.7% and 34.9% for the first thermal cycle and 42.5% to 51.5% for second thermal cycle, respectively.

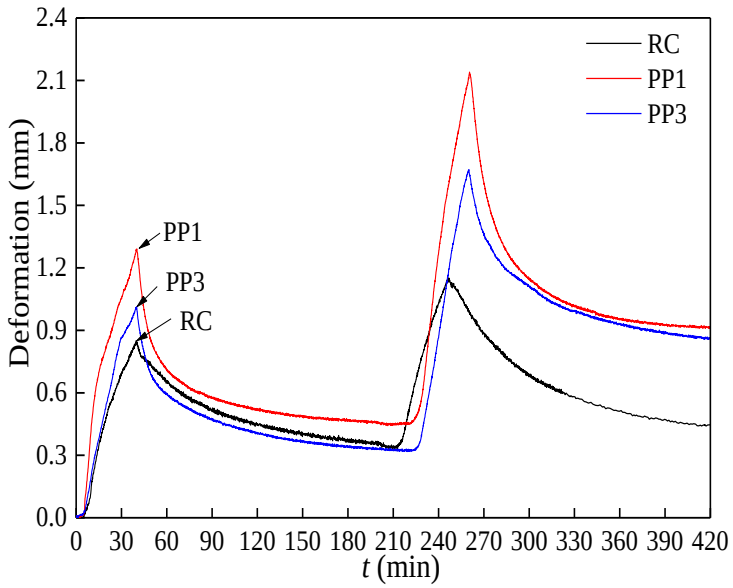

Fig.10 Comparison of the radial deformation-time curves of PP fiber reinforced and RC specimen.

Table 4. Maximum radial deformation and residual radial deformation of the pipe specimens mm

Pipe	δ_{m1}	δ_{r1}	δ_{m2}	δ_{r2}
RC	0.85	0.34	1.15	0.45
PP1	1.29	0.45	2.14	0.91
PP3	1.01	0.32	1.67	0.86
SF40	0.81	0.35	1.11	0.50
SF55	0.77	0.32	1.06	0.49
SF70	0.70	0.33	0.99	0.44
HF403	0.86	0.27	1.09	0.37
HF552	0.88	0.35	1.28	0.50
HF701	0.80	0.28	1.10	0.36

Note: δ_{m1}, δ_{m2} are the maximum d_r in the first and second thermal cycle, respectively; δ_{r1}, δ_{r2} are the d_r of the pipes at the end of first (210 mins) and second (420 mins) thermal cycle respectively.

3.1.3.2 Effect of SF on the radial deformation (d_r) of SCC pipes

Fig. 11 shows the relationship between the radial deformation (d_r) and time of SCC pipes reinforced with SF and steel mesh. In the first thermal process, the d_r increases rapidly during the first 30 mins for each cycle. The pipes of SF40, SF55 and SF70 show the similar increasing trend. The d_r of RC, SF40,

SF55, and SF70 reaches the maximum within 40 mins (at about 1000 ℃). Compared with RC specimen (0.85mm), the maximum d_r in first thermal process (δ_{m1}) of SF40 (0.81 mm), SF55 (0.77 mm) and SF70 (0.70 mm) decreased by 4.7%, 9.4% and 17.6%, respectively. During the naturally cooling stage, the d_r decreases gradually; and the d_r of the steel mesh reinforced (RC) pipe recovers more rapidly than the pipes with steel fibers. At the end of the first thermal stage, there exists a residual radial deformation (δ_{r1}) between 0.32 mm to 0.35 mm for all the RC and SF reinforced SCC pipes.

At the end of the second thermal cycle, the δ_{m2} of RC is 1.15 mm, which is 35.3% higher than that (δ_{m1}) in the first stage. In addition, this value (δ_{m2}) is 3.5%, 7.8% and 13.9% larger than that of SF40, SF55 and SF70, respectively. It means that the maximum d_r can be decreased by the addition of steel fibers. It is due to the fact that, the d_r includes both the elastic radial deformation and the plastic radial deformation, and the plastic radial deformation can be reduced by adding the SF for its excellent crack restriction ability.

After the second thermal cycle, the residual d_r (δ_{r2} is between 0.44 mm to 0.50 mm) is accumulated to a higher level than that of the first thermal cycle (δ_{r1} is between 0.32 mm to 0.35 mm), where δ_{r1} is about 41.6% - 47.1% of the δ_{m1}. For the second cycle, the value of ((δ_{r2}) /(δ_{m2})) is in the range between 44.4% and 46.2%.

From Table 4 it can be concluded that with the increasing of SF content, the residual d_r of the pipe is decreased. Compared with RC specimen, the δ_{r2} of SF40 and SF55 are increased by 11.1% and 8.9% respectively. However, the pipe specimen SF70 has the similar δ_{r2} with RC pipe (steel ratio of 0.4%). It means 70 kg/m^3 SF show a significant effect in reducing the residual radial deformation by limiting crack propagation and having a higher stiffness.

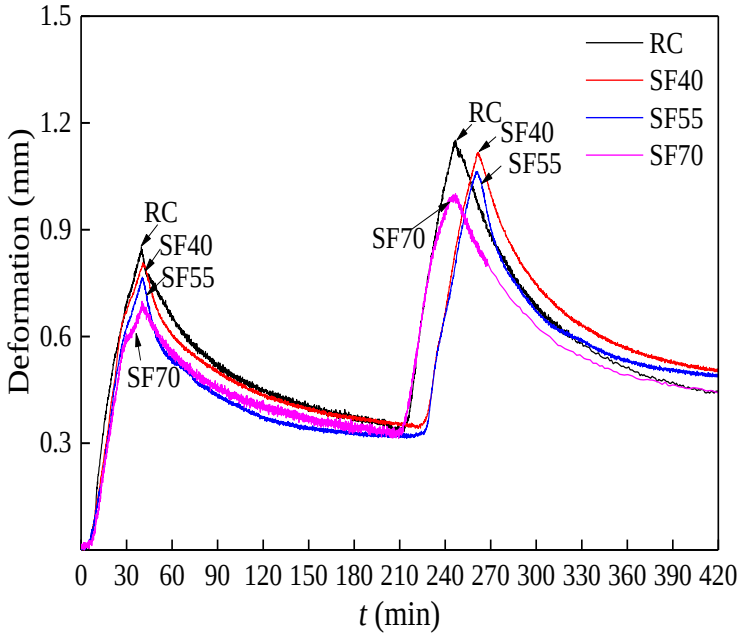

Fig.11 Comparison of radial deformation-time curves of SF reinforced and steel mesh reinforced pipe.

3.1.3.3 Effect of hybrid fiber on the radial deformation (d_r) of SCC pipes

Fig. 12 shows the comparison of the radial deformation-time curves of hybrid fiber reinforced and steel mesh reinforced RC pipe. The ascending branch of radial deformation (d_r) and time curves of hybrid fiber reinforced pipes and steel mesh pipes are very close to each other during the first heating process.

The first maximum radial deformation (δ_{m1}) of HF403 (0.86 mm) is nearly equal to that of RC specimen (δ_{m1}= 0.85 mm). However, compared with RC pipe, the peak value of first radial deformation of HF701 (δ_{m1}= 0.80 mm) decreased by 5.9%. Moreover during the second thermal cycle, the maximum d_r of HF403 (δ_{m2} =1.09 mm) and HF701 (δ_{m2} =1.10 mm) is smaller than that of RC specimen (δ_{m2} =1.15 mm). This demonstrates that the hybrid fiber reinforced pipes posses better d_r restriction ability than that of RC pipe. Moreover, the reduction of radial deformation can be mainly attributed to the addition of steel fibers.

At the end of the first naturally cooling stage (210 mins), the residual d_r of the HF403 (δ_{r1}=0.27 mm) and HF701 (δ_{r1}=0.28 mm) is less than that of RC specimen (δ_{r1}=0.34 mm). The δ_{r2}, the residual d_r at the end of the second naturally cooling stage (420 mins), of HF403 and HF701 is accumulated to 0.37 mm and 0.36 mm, respectively. Both δ_{r1} and δ_{r2} of hybrid fiber reinforced pipes are lower than those of steel mesh RC pipes, SF and PP fiber reinforced pipes. However, the pipes with mono fibers (SF or PP fiber) show a higher δ_{r2} than that of RC. The results show that the composites use of SF and

PP fibers demonstrates the positive hybrid effect on restricting the residual d_r of SCC pipes, especially in the second thermal cycle.

Compared with the residual d_r in the first thermal cycle (δ_{r1}), δ_{r2} of HF403 and HF701 are increased by 37.0% and 28.6% after two thermal cycles, respectively. The δ_{r1} is about 31.4% -35.0% of the maximum radial deformation (δ_{m1}) in the first thermal cycle, and for the second thermal cycle, the percentage of δ_{r2}/δ_{m2} is in the range between 32.7% and 33.9%. In both cycles, this percentage range of the hybrid fiber reinforced pipe is lower than that of the mono fiber reinforced pipe.

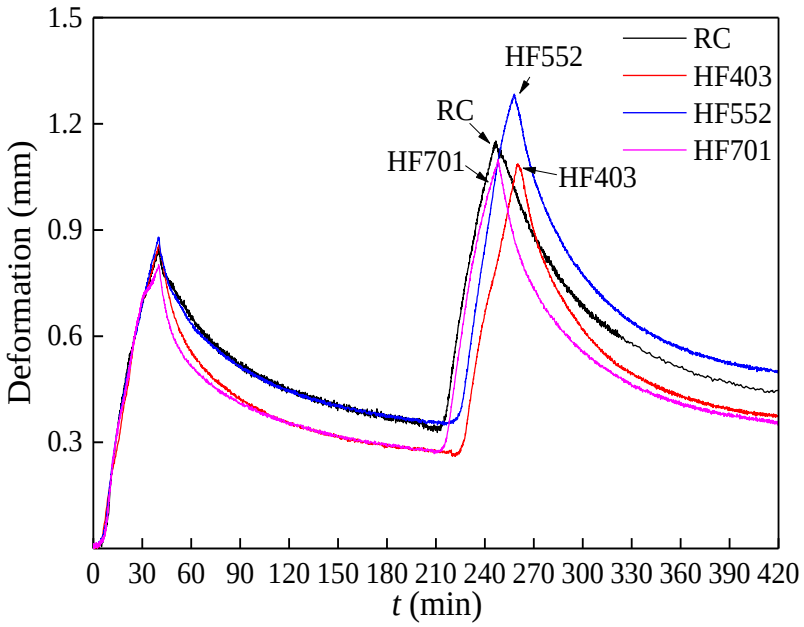

Fig.12 Comparison of the radial deformation - time curves of hybrid fiber reinforced and steel mesh reinforced pipe.

3.2. Radial deformation – temperature and radial deformation - temperature difference relationships

Fig. 13 shows the relationship between the radial deformation (d_r) and the temperature of the middle layer of the HF403 pipe. The d_r experiences two cycles along with the change of the temperature. In the first heating cycle, when the temperature of the middle layer reaches its highest value (point B, 154.8 ℃, 0.78 mm) the radial deformation does not achieve the maximum value (at point A, 145.8 ℃,

0.86 mm). Similarly, in the second thermal cycle, the maximum radial deformation (point C, 218.1 ℃, 1.09 mm) also does not coincide with the highest temperature (point D, 228.1 ℃, 0.96 mm). Fig. 14 shows the relationship between the radial deformation of the pipe and the temperature difference (Δ_T) between the inside layer and the outside layer of the HF403 pipe. In the two thermal processes, the d_r reaches the maximum when the Δ_T reaches the highest value [point E (352.5 ℃, 0.86 mm) for the first and point F (330.5 ℃, 1.09 mm) for the second cycle]. Similar phenomenon can be found in other specimens as well. Combined with Fig.13 and Fig. 14, it can be seen that the temperature difference has a stronger effect on the radial deformation than that of the temperature for SCC pipes, and the temperature difference is the major influence factor for the radial deformation.

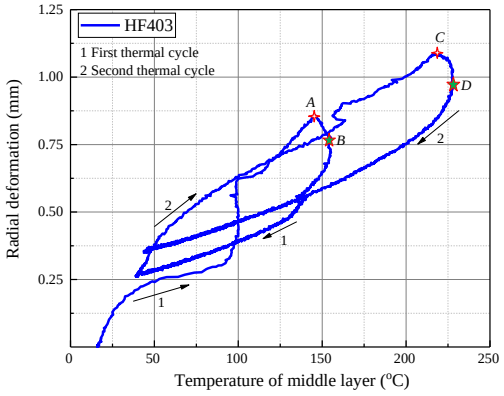

Fig. 13 Radial deformation-temperature curve.

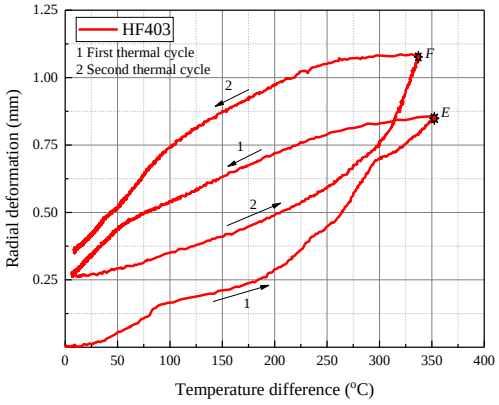

Fig. 14 Radial deformation-temperature difference curve.

3.3. Simplified calculation method of the radial deformation under the thermal

As mentioned in the introduction, one of the purposes of this work is to explore a simplified calculation method for estimating the portion of the elastic radial deformation in the total radial

deformation. The total radial deformation includes two parts: the elastic radial deformation, and the plastic radial deformation. A closed-form analytical solution with differential equation for non-elastic state is very complicated and tedious for engineering practice.

From the experimental results, the maximum d_r of the pipes increases with the number of cycles, but the major portion of the d_r develops during the first thermal cycle (the average value of δ_{m1}/δ_{m2} is 0.70), so it is reasonable to evaluate the maximum d_r in the first cycle. In order to analyze the maximum d_r of the pipe specimens in the first thermal cycle, the elastic radial deformation should be firstly evaluated, and then its proportion in total deformation will be analyzed. Assuming that in the stable phase of the gas temperature, the thermal stress of the pipe can be calculated according to the plane strain problem based on the elasticity theory. Parameter a and b are the radius of the inside layer and outside layer of the concrete pipe, respectively; T_a and T_b are the temperatures change of the pipe inside and pipe outside layers, respectively and E, μ and α are the elastic modulus after first thermal exposure, the Poisson's ratio and the thermal expansion coefficient, respectively. Additionally, the thermal expansion coefficient of concrete is tested according to the Standard AASHTO T 336-11[35]. For the temperature stress of the thin-shell cylinder in two-dimensional temperature field, the expressions in the polar coordinates are given as follows:

Radial stress:

$$\sigma_r = -\frac{E\alpha(T_a - T_b)}{2(1-\mu)}\left(\frac{\ln\frac{b}{r}}{\ln\frac{b}{a}} - \frac{\frac{b^2}{r^2}-1}{\frac{b^2}{a^2}-1}\right) \qquad \text{Eqn.(1)}$$

Hoop stress:

$$\sigma_\theta = -\frac{E\alpha(T_a - T_b)}{2(1-\mu)}\left(\frac{\ln\frac{b}{r}-1}{\ln\frac{b}{a}} + \frac{\frac{b^2}{r^2}+1}{\frac{b^2}{a^2}-1}\right) \quad \text{Eqn. (2)}$$

The radial strain (ε_r) is given in equations (3):

$$\varepsilon_r = \frac{(1-\mu^2)}{E}\left(\sigma_r - \frac{\mu}{1-\mu}\sigma_\theta\right) + (1+\mu)\alpha T \quad \text{Eqn. (3)}$$

where

$$T = T_a\frac{\ln\frac{b}{r}}{\ln\frac{b}{a}} + T_b\frac{\ln\frac{a}{r}}{\ln\frac{a}{b}} \quad \text{Eqn. (4)}$$

Replace Eqns.(1), (2) and (4) in (3), ε_r can be obtained. The radial deformation δ_c is calculated in Eqn.(5) :

$$\delta_c = \int_a^b \varepsilon_r dr\,. \quad \text{Eqn. (5)}$$

The elastic modulus, the Poisson's ratio and the thermal expansion coefficient are listed in Table 5.

Table 5 Elastic modulus, Poisson's ratio and thermal expansion coefficient of the concrete, and temperature change of the pipes

Specimen	E(GPa)	μ	α ($10^{-6}\cdot$℃$^{-1}$)	T_a(℃)	T_b(℃)
PC	8.88	0.2	7.52	405.3	98.1
PP1	6.72	0.2	7.16	420.8	78.1
PP3	6.62	0.2	5.89	401.8	91.1
SF40	9.28	0.2	7.21	399.6	81.9
SF55	8.87	0.2	7.73	437.1	99.4
SF70	8.44	0.2	6.96	368.0	88.6
HF403	7.15	0.2	5.57	430.5	81.4
HF552	8.60	0.2	6.05	374.4	79.5
HF701	8.51	0.2	6.99	315.4	73.3

The elastic radial deformation and measured radial deformations of the first thermal stage are listed in Table 6, it can be seen that the calculated elastic radial deformation (δ_c) is 15.5 - 25.9% of the maximum radial deformations in the first thermal cycle (δ_{m1}). The average elastic radial deformation (δ_c) is 22.3% of the maximum radial deformation in the first thermal cycle (δ_{m1}) of all the specimens.

The average δ_{r1} of the first thermal process was about 0.333 mm (see Table 6). Furthermore the elastic radial deformation (δ_c) is more than a half of the average δ_{r1} in the first thermal cycle for all the pipes (δ_c /δ_{r1}= 0.582). The standard deviation (S.D.) of δ_c /δ_{m1} is 0.054, which is very small. It means the proportion of elastic radial deformation can be predicted stable.

Based on the observed experimental results and the elastic calculation, a simplified method for estimating the maximum radial deformation of fiber reinforced SCC pipe members for engineering practice is suggested in Eqn. (6).

$$\delta_{m1} = \varphi(2.32\delta_c + 0.333) \qquad \text{Eqn. (6)}$$

where φ is the fiber effect coefficient, according to the fitting analysis result (R^2= 0.92), φ is 1.0, 1.5, 1.0 and 1.2 for the pipes reinforced with steel mesh, PP fiber, SF and hybrid fibers, respectively.

Table 6. Measured and theoretical calculated radial deformations of the pipes

Pipes	Measured values				Calculated values				
	δ_{m1} (mm)	δ_{m2} (mm)	δ_{r1}(mm)	δ_{r2}(mm)	δ_c (mm)	δ_c /δ_{m1}	δ_c /δ_{m2}	δ_c /δ_{r1}	δ_c /δ_{r2}
RC	0.85	1.15	0.34	0.45	0.22	0.259	0.191	0.647	0.489
PP1	1.29	2.14	0.45	0.91	0.2	0.155	0.093	0.444	0.220
PP3	1.01	1.67	0.32	0.86	0.17	0.168	0.102	0.531	0.198
SF40	0.81	1.11	0.35	0.5	0.2	0.247	0.180	0.571	0.400
SF55	0.77	1.06	0.32	0.49	0.24	0.312	0.226	0.750	0.490
SF70	0.7	0.99	0.33	0.44	0.18	0.257	0.182	0.545	0.409
HF403	0.86	1.09	0.27	0.37	0.16	0.186	0.147	0.593	0.432
HF701	0.8	1.1	0.28	0.36	0.16	0.200	0.145	0.571	0.444
Average	0.886	1.289	0.333	0.548	0.191	0.223	0.158	0.582	0.385

S.D.	0.186	0.403	0.055	0.215	0.029	0.054	0.045	0.089	0.114

In the second thermal cycle, the d_r is increased compared with that in the first cycle, because the inelastic deformation and the crack development of concrete become stronger than that in the first thermal cycle. Thus, the average of δ_c /δ_{m2} is decreased to 15.8%. In addition, the average δ_{r2} is 0.548 mm, which is 2.87 times as much as the average δ_c, and the S.D. of δ_c /δ_{r2} is a little larger than that of δ_c /δ_{r1}, which may be caused by the different crack restriction effect of the fibers during the second thermal cycle.

4. Conclusions

The experimental and analytical results have led to the following conclusions:

- The temperature difference has stronger influence on the radial deformation than that of the temperature for SCC pipes. The experimental results demonstrate that the radial deformation reaches the maximum when the temperature difference reaches the maximum. However, the maximum radial deformation and the maximum temperature do not happen at the same time.

- The test results indicate that the inclusion of PP fiber and SF reduces the temperature difference Δ_T between the inside layer and outside layer significantly, and the higher fiber content leads to a more uniform temperature field in the pipes than that of pipes with lower fiber content.

- The addition of micro PP fiber and macro SF plays some roles in reducing the radial deformation in the SCC pipes exposed to fire. Compared with the mono fiber, the composed use of micro PP fiber and SF indicates the positive hybrid effect on the residual radial deformation reduction of the SCC pipes subjected to fire.

- The test results show that the calculated elastic radial deformation is between 15.5% and 25.9% (with an average value of 22.3%) of the total radial deformation of the SCC pipes in the first

thermal cycle. A simplified method for estimating the maximum radial deformation in the first thermal cycle of fiber reinforced SCC pipe members for engineering practice is suggested.

Acknowledgments

The authors acknowledge the National Natural Science Foundation of China (Grant: 51578109).

References

[1] BANGI M R, HORIGUCHI T. Pore pressure development in hybrid fibre-reinforced high strength concrete at elevated temperatures [J]. Cement & Concrete Research, 2011, 41(11): 1150-6.
[2] BRANDT A M. Fibre reinforced cement-based (FRC) composites after over 40 years of development in building and civil engineering [J]. Composite Structures, 2008, 86(1): 3-9.
[3] MOHAMED N, SOLIMAN A M, NEHDI M L. Mechanical performance of full-scale precast steel fibre-reinforced concrete pipes [J]. Engineering Structures, 2015, 84:287-99.
[4] SAVOV K, LACKNER R, MANG H A. Stability assessment of shallow tunnels subjected to fire load [J]. Fire Safety Journal, 2005, 40(8): 745-63.
[5] BANTHIA N, SAPPAKITTIPAKORN M. Toughness enhancement in steel fiber reinforced concrete through fiber hybridization [J]. Cement and Concrete Research, 2007, 37(9): 1366-72.
[6] DING Y, YOU Z, JALALI S. Hybrid fiber influence on strength and toughness of RC beams [J]. Composite Structures, 2010, 92(9): 2083-9.
[7] Bao J, Li S, Zhang P, et al. Influence of the incorporation of recycled coarse aggregate on water absorption and chloride penetration into concrete[J]. Construction and Building Materials, 2020, 239: 117845.
[8] BURATTI N, MAZZOTTI C, SAVOIA M. Post-cracking behaviour of steel and macro-synthetic fibre-reinforced concretes [J]. Construction and Building Materials, 2011, 25(5): 2713-22.
[9] KALIFA P, MENNETEAU F D, QUENARD D. Spalling and pore pressure in HPC at high temperatures [J]. Cement & Concrete Research, 2000, 30(12): 1915-27.
[10] Bao J, Xue S, Zhang P, et al. Coupled effects of sustained compressive loading and freeze–thaw cycles on water penetration into concrete[J]. Structural Concrete, 2020.
[11] DING Y, AZEVEDO C, AGUIAR J B, et al. Study on residual behaviour and flexural toughness of fibre cocktail reinforced self compacting high performance concrete after exposure to high temperature [J]. Construction & Building Materials, 2012, 26(1): 21-31.
[12] HAKTANIR T, ARI K, ALTUN F, et al. A comparative experimental investigation of concrete, reinforced-concrete and steel-fibre concrete pipes under three-edge-bearing test [J]. Construction & Building Materials, 2007, 21(8): 1702-8.
[13] PARK Y, ABOLMAALI A, BEAKLEY J, et al. Thin-walled flexible concrete pipes with synthetic fibers and reduced traditional steel cage [J]. Engineering Structures, 2015, 100: 731-41.
[14] OZAWA M, UCHIDA S, KAMADA T, et al. Study of mechanisms of explosive spalling in high-strength concrete at high temperatures using acoustic emission [J]. Construction & Building Materials, 2012, 37(3): 621-8.
[15] TOROPOVS N, MONTE F L, WYRZYKOWSKI M, et al. Real-time measurements of temperature, pressure and moisture profiles in High-Performance Concrete exposed to high temperatures during neutron radiography imaging [J]. Cement & Concrete Research, 2015, 68:166-73.
[16] DING Y, ZHANG C, CAO M, et al. Influence of different fibers on the change of pore pressure of self-consolidating concrete exposed to fire [J]. Construction & Building Materials, 2016, 113:456-69.
[17] ZEIML M, LEITHNER D, LACKNER R, et al. How do polypropylene fibers improve the spalling behavior of in-situ concrete? [J]. Cement & Concrete Research, 2006, 36(5): 929-42.
[18] KODUR V K R, CHENG F-P, WANG T-C, et al. Effect of Strength and Fiber Reinforcement on Fire Resistance of High-Strength Concrete Columns [J]. Journal of Structural Engineering, 2003, 129(2): 253-9.

[19] Abdulhaleem K N, Gülşan M E, Çevik A. Mechanical behavior of steel fiber‐reinforced self‐compacting concrete corbels after exposure to elevated temperatures[J]. Structural Concrete, 2018, 19(6): 1881-1894.
[20] ALTUN F, HAKTANIR T, ARI K. Effects of steel fiber addition on mechanical properties of concrete and RC beams [J]. Construction & Building Materials, 2007, 21(3): 654-61.
[21] MASHIMO H. State of the road tunnel safety technology in Japan [J]. Tunnelling & Underground Space Technology Incorporating Trenchless Technology Research, 2002, 17(2): 145-52.
[22] KHALIQ W, KODUR V. Thermal and mechanical properties of fiber reinforced high performance self-consolidating concrete at elevated temperatures [J]. Cement & Concrete Research, 2011, 41(11): 1112-22.
[23] LAU A, ANSON M. Effect of high temperatures on high performance steel fibre reinforced concrete [J]. Cement & Concrete Research, 2006, 36(9): 1698-707.
[24] YERMAK N, PLIYA P, BEAUCOUR A L, et al. Influence of steel and/or polypropylene fibres on the behaviour of concrete at high temperature: Spalling, transfer and mechanical properties [J]. Construction & Building Materials, 2017, 132: 240-50.
[25] BYRNE EMMA G K, CARVEL RICKY. Fires in Ducts: A review of the early research which underpins modern tunnel fire safety engineering [J]. Tunnelling and Underground Space Technology 2018, 81: 306-314.
[26] YU L X, LIU F, LIU Y Q, et al. Experimental study on thermal and smoke control using transverse ventilation in a sloping urban traffic link tunnel fire [J]. Tunnelling & Underground Space Technology, 2018, 71:81-93.
[27] KEREKES Z, LUBL Y É, REST S Á. Standard fire testing of Chimney Linings from Composite Materials [J]. Journal of Building Engineering, 2018, 19: 530-538.
[28] Specification and Guidelines for Self-Compacting Concrete. EFNARC 2002
[29] DING YINING, GANG QUAN, DONG XIANGJUN, et al. A kind of chrome-nickel or nickel steel fabricated high-temperature deformation sensor : China, 200410100477.3[P].2004-12-23.
[30] Ingason H, Li Y Z, Lönnermark A. Tunnel fire dynamics[M]. Springer, 2014.
[31] ISO 834-1-1999. Fire-resistance test-Elements of building construction-Part 1: General requirements [S]. International Organization for Standardization,1999.
[32] EN 1363- 1: 2012. Fire Resistance Tests–Part 1: General Requirements [S]. European Committee for Standardization, 2012.
[33] UNI EN 13216-1:2006. CHIMNEYS - TEST METHODS FOR SYSTEM CHIMNEYS - PART 1: GENERAL TEST METHODS [S]. Italy; Ente Nazionale Italiano di Unificazione (UNI). 2006.
[34] KALIFA P, CH N G, GALL C. High-temperature behaviour of HPC with polypropylene fibres: From spalling to microstructure [J]. Cement & Concrete Research, 2001, 31(10): 1487-99.
[35] AASHTO T. 336-11. Coefficient of Thermal Expansion of Hydraulic Cement Concrete [S].

American Association of State Highway and Transportation Officials, 2011.

Table 1. Base mixture proportion of plain concrete (kg/m^3)

Cement	Fly ash	Fine aggregate (0-5 mm)	Coarse aggregate (5-12 mm)	Water	Superplasticizer	Water/Binder
500	100	764	764	222	3.5	0.37

Table 2. Properties of steel fiber and polypropylene fiber

Fiber	Length (mm)	Diameter(mm)	Tensile stress(MPa)	Pieces for per kilogram	Melting Point(℃)
PP fiber	15	0.03	400	2×10^7	165
SF	35	0.55	1200	15000	1500

Table 3. Fiber dosages, slump flow and compressive strength of FRC

Specimen	PP fiber(kg/m^3)	SF(kg/m^3)	Slump flow(cm)	Compressive stress(MPa)
RC	0	0	68	43.6
PP1	1	0	55	38.9
PP3	3	0	39	37.6
SF40	0	40	64	48.2
SF55	0	55	62	47.5
SF70	0	70	59	45.9
HF403	3	40	37	38.1
HF552	2	55	48	41.9
HF701	1	70	52	42.6

Table 4. Maximum radial deformation and residual radial deformation of the pipe specimens mm

Pipe	δ_{m1}	δ_{r1}	δ_{m2}	δ_{r2}
RC	0.85	0.34	1.15	0.45
PP1	1.29	0.45	2.14	0.91
PP3	1.01	0.32	1.67	0.86
SF40	0.81	0.35	1.11	0.50
SF55	0.77	0.32	1.06	0.49
SF70	0.70	0.33	0.99	0.44
HF403	0.86	0.27	1.09	0.37
HF552	0.88	0.35	1.28	0.50
HF701	0.80	0.28	1.10	0.36

Note: δ_{m1}, δ_{m2} are the maximum d_r in the first and second thermal cycle, respectively; δ_{r1}, δ_{r2} are the d_r of the pipes at the end of first (210 mins) and second (420 mins) thermal cycle respectively.

Table 5. Elastic modulus, Poisson's ratio and thermal expansion coefficient of the concrete, and temperature change of the pipes

Specimen	E(GPa)	μ	α ($10^{-6}\cdot℃^{-1}$)	T_a(℃)	T_b(℃)
PC	8.88	0.2	7.52	405.3	98.1
PP1	6.72	0.2	7.16	420.8	78.1
PP3	6.62	0.2	5.89	401.8	91.1
SF40	9.28	0.2	7.21	399.6	81.9
SF55	8.87	0.2	7.73	437.1	99.4
SF70	8.44	0.2	6.96	368.0	88.6
HF403	7.15	0.2	5.57	430.5	81.4
HF552	8.60	0.2	6.05	374.4	79.5
HF701	8.51	0.2	6.99	315.4	73.3

Table 6. Measured and theoretical calculated radial deformations of the pipes

Pipes	Measured values				Calculated values				
	δ_{m1} (mm)	δ_{m2} (mm)	δ_{r1}(mm)	δ_{r2}(mm)	δ_c (mm)	δ_c/δ_{m1}	δ_c/δ_{m2}	δ_c/δ_{r1}	δ_c/δ_{r2}
RC	0.85	1.15	0.34	0.45	0.22	0.259	0.191	0.647	0.489
PP1	1.29	2.14	0.45	0.91	0.2	0.155	0.093	0.444	0.220
PP3	1.01	1.67	0.32	0.86	0.17	0.168	0.102	0.531	0.198
SF40	0.81	1.11	0.35	0.5	0.2	0.247	0.180	0.571	0.400
SF55	0.77	1.06	0.32	0.49	0.24	0.312	0.226	0.750	0.490
SF70	0.7	0.99	0.33	0.44	0.18	0.257	0.182	0.545	0.409
HF403	0.86	1.09	0.27	0.37	0.16	0.186	0.147	0.593	0.432
HF701	0.8	1.1	0.28	0.36	0.16	0.200	0.145	0.571	0.444
Average	0.886	1.289	0.333	0.548	0.191	0.223	0.158	0.582	0.385
S.D.	0.186	0.403	0.055	0.215	0.029	0.054	0.045	0.089	0.114